

sediment structure are not observed anywhere for any fault block within the intraplate deformation area in the CIB till now.

The central high appears to be bound in north and south by steep fault scarps running through sediments. The faults seem to be relatively young and the eastern and western flanks of the high reveal a gradual slope (Fig. 7.12a and 7.12b). This may indicate an older age for the fracture zones which seem to bound this block from east and west. The eastern slope is more steeper than in the west and shows very clearly that upper syn-deformation sediments unconformably lap on to lower pre-deformation strata.

The northern high at the polygon S22-II is nearly in isometrical form, about 150 x 160 km in visible size as compared with 100 x 135 km size of its topographic expression (Chapter 3). Figures 7.12c and 7.12d show SW-NE and NE-SW cross-sections respectively. Morphology of bottom relief and inner structure of pre-deformation sediments are different here from those in other fault blocks studied previously (and at the polygon S22-II discussed above). On the northern high, one can see both large regular asymmetric folds and small-scale block faulting. The folds are observed mostly on the eastern flank of the northern high and partly on the western flank too, while its entire central part reveals the small-scale block faulting.

Based on the seismic reflection profiles alone, preparation of any structural map for the polygon S22-II is not possible because basement and reflector 'A' are not recorded clearly due to widely-spaced profiles across the rises where syn-deformation and post deformation sediments exist. This upper unit reaches up to 0.8s thick in the depressions and terminates by pinching out against the foothill of rises that are carpeted by pre-deformation sediments.

### THE S22 CRUISE 30 L AIRGUN SOURCE SEISMIC REFLECTION STUDIES

In Leg 2 of the S22 cruise single-channel seismic reflection digital data with a 30 l airgun source were collected along five regional lines totalling 1150 km and in polygon S22-III in the equatorial region of the CIB, between 2° N and 2° S, 81°25' E and 81°45' E (Fig. 7.13, Figs. 2.4 and 2.7). Some 0.3 l airgun seismic reflection profiles were also collected here. The digital seismic reflection data were processed at National Institute of Oceanography, Goa using the "NORSEIS" package of Geco Mapping System, Norway (NORSEIS, 1988). The processing operations mainly removed the random noise (MUTE). Filters with 8-40 Hz band width were used after several trials with other frequency settings as well as other types of filters such as space and time variant filter (STVF), F-K dip filter etc. Predictive deconvolution with an auto correlation window of 200 ms and prediction lag of 8 ms were used to improve the signal to noise ratio (Murthy et al. 1993b).

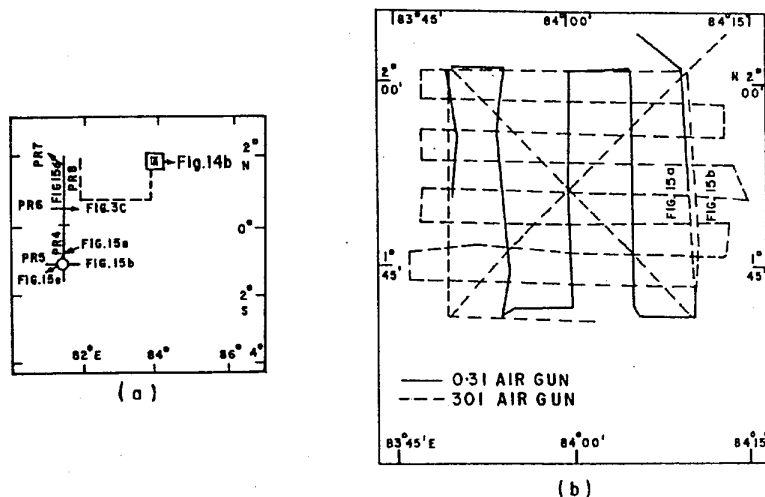


Fig. 7.13. The S22 cruise track maps of (a) 30 l airgun source profiles and (b) the polygon S22-III survey.

Three N-S trending seismic profiles (Fig 7.13a, Profile. 4, 7 and 8) were collected during the Leg 2 of the cruise with 30 l airgun source. Profile 4 between equator and 2°S, paralleling 81°25'E passes over the ODP sites 717 to 719. Profile 7 is its northern continuation from equator to 2°N. The N-S trending profile following 81°25' E is about 460 km. long. Profile 8 is parallel to profile 7 and follows 81°45' E. The E-W trending profile 5 along 1° S passes over the ODP site 718. Profile 6 along 0°30' N runs parallel to profile 5.

Processed and interpreted seismic sections along part of profiles 4 to 7 are shown in Figures 7.14a to 7.14e. Here depth to the seabed varies from 5.9 to 6.6s with higher depths observed in the southern part compared to the northern part. Depths are also higher over the western part compared to the eastern part. The topography is in general flat and devoid of any significant features, with the exception of some U-shaped turbidity channels (Fig. 7.14d, profile 7, shot points 1 to 100). Surface expression of deformation is observed at two places, south of equator (0°18' S, Fig 7.14a, profile 4, shot points 400-600 and 1° S, Fig 7.14e, profile 4, shot points 200-250).

Acoustic basement is observed at depths varying from 8.5 to 8.9s (Fig. 7.14a to e). While water depth increases from north to south, the basement is more or less at constant depth, thereby suggesting a decrease in sediment thickness towards south. Seismic sections along profiles 6 and 7 indicate that the basement in the north-western part of the study area between 2° N and equator is folded and faulted. Whereas the overlying sediments are unaffected. In contrast, the basement and the overlying sediments in the southern part from equator to 1°30' S are severely folded and faulted.

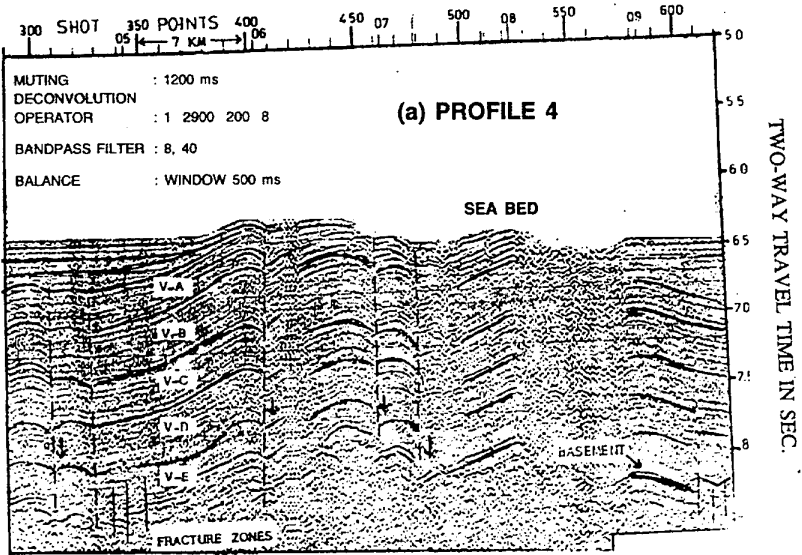


Fig.7.14a.

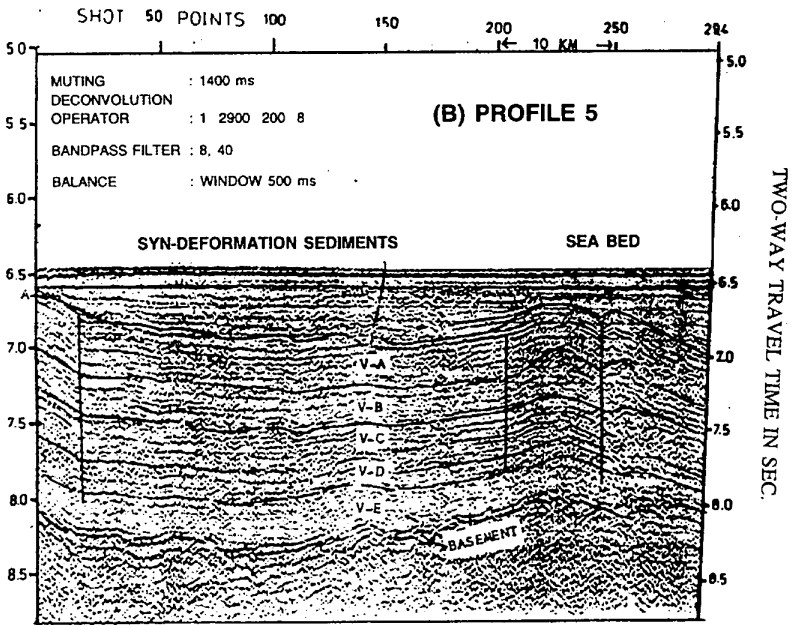


Fig.7.14b.

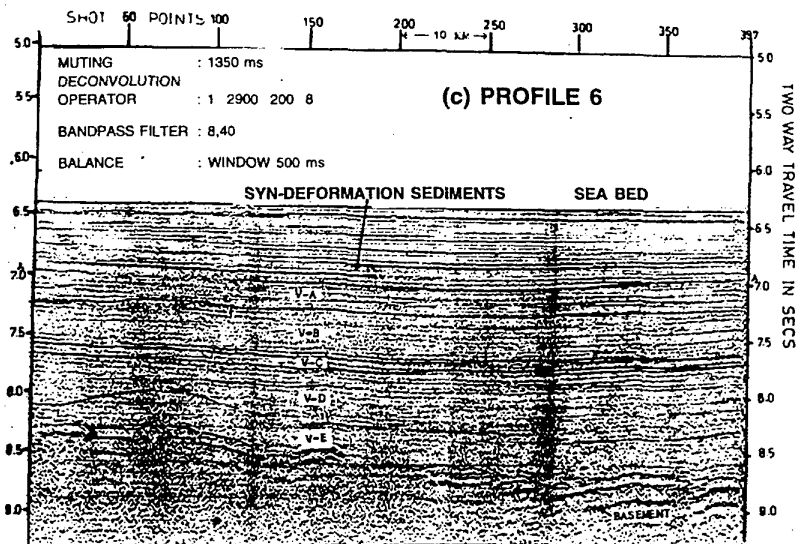


Fig.7.14c.

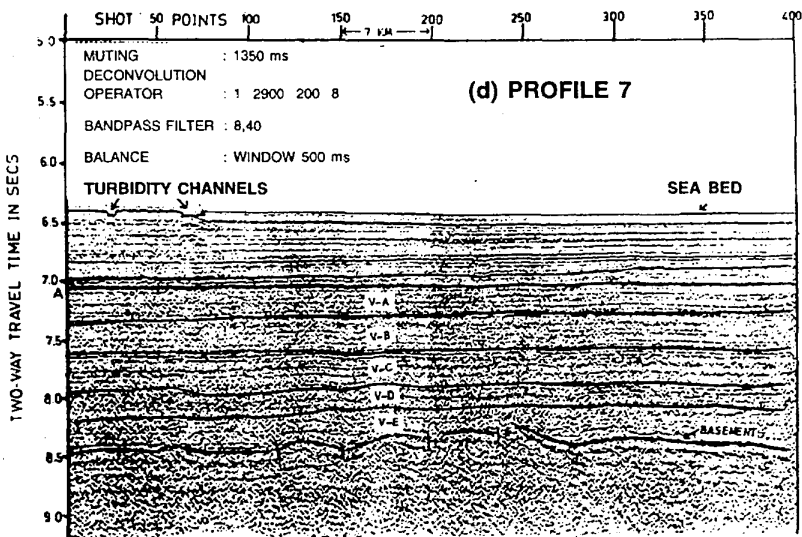


Fig.7.14d.

A series of anticlinal folds separated by synclinal basins are more deformed along profile 4 and two of them outcrop at 0°10' S, 81°25' E (Fig

7.14a, shot points 400-600). The ODP sites 717 to 719 are located over the faulted and uplifted blocks near  $1^{\circ}$  S (Fig 7.14e, shot points 1 to 250), which represent the short wavelength expression of the intraplate deformation.

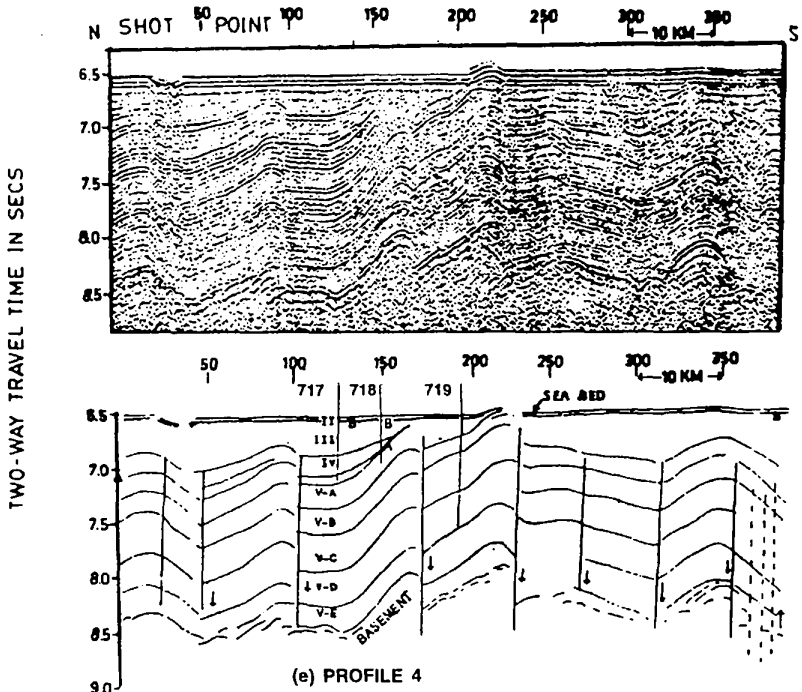


Fig. 7.14 a to e. Processed seismic reflection profiles of the 30 l airgun source from the S22 cruise. Location of the profiles is shown in Fig. 7.13a.

The wavelength of deformed folds is of the order of 50 km, having an amplitude of the order of 0.5s (approximately 500 m). The deformed blocks are bound by near vertical faults (Figs. 7.14a, e). Most of these faults display a downthrow towards south. They are more prominent and closely spaced near the anticlinal folds compared to the synclinal basins where they are relatively less and widely spaced. The faulted blocks show relatively steep dip on the northern side, whereas they dip gently to form synclinal basins towards south (Fig. 7.14e). The close faulting observed in the basement at some places ( $0^{\circ}36'$  S and  $0^{\circ}15'$  S, Fig 7.14a, shot points 300-350) is not reflected in the overlying sediments. These faults appear to be unrelated to the process of the recent intraplate deformation and might represent pre-existing fracture zones that are much older than the near vertical faults associated with the deformed blocks.

The present data indicate sediment thickness varying from 1.5 to 2.2s in the southern part and from 2.3 to 2.8s in the northern part. Two prominent

unconformities 'A' and 'B' (Fig. 7.14) can be traced within the sedimentary section. The lower unconformity 'A' separates the younger syn-deformation sediments from the older pre-deformation sediments and thus mark the onset of intraplate deformation since late Miocene. This unconformity becomes conformable near the synclinal basins away from the faulted blocks.

The thickness of the pre-deformation sediments in the present study area varies from 1.2 to 1.4s and the individual units are parallel, well stratified and uniform in thickness. They follow the general trend of the basement even at the crests of the faulted, deformed blocks. The syn-deformation sediments above unconformity 'A' lap onto the pre-deformation sediments. The reflectors within the syn-deformation sediments pinch out towards the top of the faulted blocks. The thickness of the syn-deformation sediments is about 0.8s near the synclinal basins (near site 717, Fig. 7.14e) away from the faulted uplifted blocks. While it reduced nearly to 0.1s over the crests of the faulted blocks (site 718, Fig. 7.14e). The upper unconformity 'B' is undulating in nature and it is basically a surface separating flat-lying reflectors from the underlying tilted or undulating reflectors. It was interpreted by Cochran (1990) as an erosional unconformity related to glacial-nonglacial sea level variations during the upper Pleistocene period (800 Ka). Sediments above this unconformity are mostly horizontal.

Seismic reflection data along profiles 4 to 8 suggest five units of fan turbidites as reported earlier by Cochran (1990), though Unit I is not clearly traceable in the 30 l airgun records. Further, the present data indicate five subunits within Unit V (Fig. 7.14e) separated by depositional unconformities having strong reflection character. The thicknesses of these subunits are as follows:

Sub units of V	Average thickness in sec TWT
V-A	0.16
V-B	0.24
V-C	0.32
V-D	0.32
V-E	0.16
Total :	1.20

Our seismic records (Fig. 7.14e) indicate that the two lowermost subunits (V-D and V-E) are located below the base of the ODP site 718 (Murthy et al. 1993b). They may be the fan turbidites and their age in this area is older, probably Oligocene (23 Ma). To predict the age, the early Miocene average sedimentation rate reported by Cochran (1990) was extrapolated downwards.

The subunit V-E draping the acoustic basement is different in seismic character, absence of layering and transparent in nature compared to the overlying turbidite sequence (Figs. 7.14b, c, e). Curray and Moore (1971) reported a similar unit of transparent sediments (not turbidite and pelagic in nature) above the basement in the Bengal Fan and interpreted them as a sequence of pre-fan sediments. Moore et al. (1974) traced this unit and the

unconformity separating it from the overlying sediments from seismic records on the western flank of the Ninetyeast Ridge and concluded that the unconformity coincides with hiatus between Paleocene and middle Eocene. Curray and Munasinghe (1989) reported the occurrence of this Eocene unconformity over much of the Bengal Fan between 2° N and 10° N.

Our seismic data along profiles 4 to 8 indicate that the Eocene unconformity and the visible pre-fan sediments below the turbidite sequence could extend southwards up to 1° S.

### **Polygon S22-III**

Seismic reflection profiles were collected with both 30 l and 0.3 l airgun sources over the small detailed area 45 x 45 km Polygon S2-III centred around 1°50' S and 84° E just north-east of the polygon S22-II. It was chosen for seismic tomography experiment of the crust with OBS's network (Figs 2.4 and 2.7), because mainly E-W trending 30 l airgun profiles 35-50 km long spaced at 5 km interval cover in grid about 600 sq. km area here. Detailed cruise tracks of the polygon S22-III are shown in Figures 2.7 and 7.13b.

Along N-S trending profiles seismic reflection data in both analog and digital form of about 200 line km using 0.3l airgun source were collected at this area to study upper part of sedimentary cover. The digital seismic data were processed at NIO. Figure 7.15 shows part of the processed seismic reflection profile and the structure of sedimentary cover in polygon does not differ much from the one already described above.

The polygon S22-III area seems to cover the western part of some domal basement high (fault block) whose visible amplitude is up to 0.8s (Fig. 7.15a). Both basement and most of the overlying sediments are deformed and buried by flat-layered undeformed sediments. N-S trending seismic reflection profiles, especially in the eastern part of the polygon clearly show that distinct folds superpose basement high. While E-W trending profiles did not reveal such folds.

Unconformity 'A' is clearly visible only near the crests of the folds, because seismic reflectors within upper relatively undeformed sediments pinch out towards the crests of folds and unconformably lap on to lower deformed sediments. But it is almost indistinguishable throughout synclinal basins. In general, unconformity 'A' and seismic reflectors within the pre-deformation sedimentary sequence below it are parallel to each other and to the basement. The sequence of 1.7-2 km thickness is reduced over the basement highs. It is a layer of strong reflection above and acoustically more transparent below, changing gradually downwards.

On the seismic records packets of short strong reflectors are revealed at the base of the sequence. They could be traced through, upto tens of kilometers, unconformably lap on to flanks of ancient basement highs and

are parallel to unconformity 'A' in general. These reflectors were interpreted as the lowest sedimentary unit draping basement. So, this unit should be represented by pre-fan pelagic sediments and, therefore, its erosional top

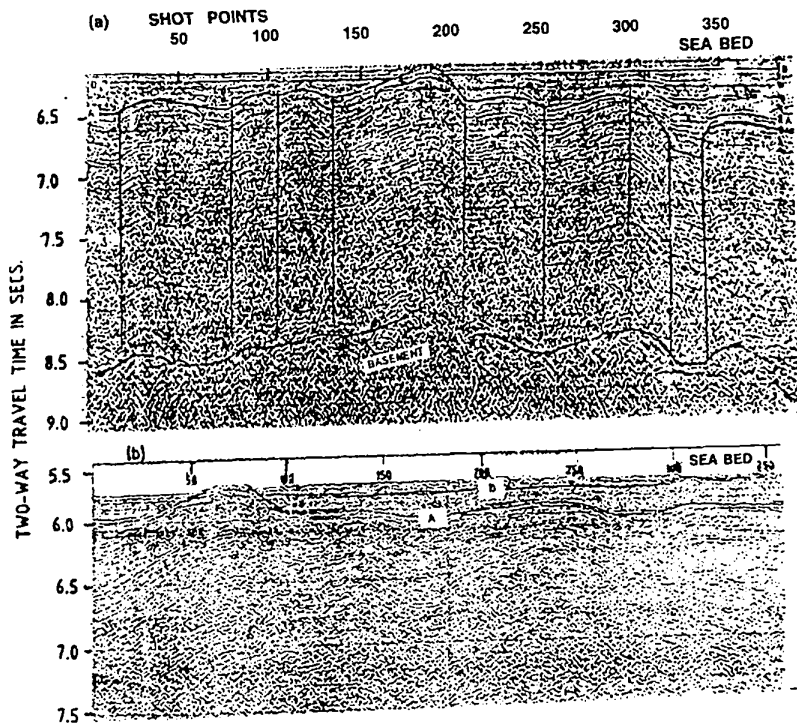


Fig. 7.15. Processed seismic reflection profiles from the polygon S22-III carried out by means of (a) 30 l and (b) 0.3 l airgun sources (location in Fig. 7.13b).

could be inferred as the Eocene unconformity discussed above. The unit appears to be layered at the polygon S22-III. In other areas it was transparent in nature. The local geological conditions might have contributed for resolution of 30 l airgun source.

On the high-resolution 0.3 l airgun seismic records upper unconformity 'B' is distinct everywhere at the polygon S22-III (Fig. 7.15b). It occurs at maximum depth of 0.22s below sea bed.

Seismic reflectors above the unconformity 'B' are essentially flat-lying. The faulted block is totally covered by the post-deformation sediments except on an arch of high where deformed sediments crop out at the sea floor with elevation of about 40 m.

Within syn-deformation sedimentary sequence between unconformities 'A' and 'B' seismic reflectors follow the structural pattern of underlying



unconformity 'A' and deeper reflectors. Moreover, their slope appears to decrease gradually upwards. Buried channels characteristic of the fan turbidite sequence are distinguished within the sedimentary sequence above unconformity 'A' and mostly above unconformity 'B'. No such characteristics are seen within sedimentary sequence below unconformity 'A'.

Isopach maps were prepared from the seismic reflection profiles collected at the polygon (Murthy et al. 1993b). They represent total sediment thickness above the acoustic basement, sediment thickness above the late Miocene unconformity 'A' and thickness of basal pre-fan sediments below the Eocene unconformity draping basement (Fig. 7.16a, b and c).

The total sediment thickness varies from 2s near the crest of the fault block in the eastern part to 3s in basal parts in the west. Thickness of syn-deformation and post-deformation sediments above unconformity 'A' varies from nearly 0.0s over the crest of the deformed block to about 0.8s over the basal part. The deformed block is completely overlain by these sediments except in the eastern part where the unconformity 'A' outcrops.

The NE-SW trending tectonic features are clearly seen in both the isopach maps. The fault block manifesting itself as basement high comprises of some NE trending folds 15-25 km long involving sediments up to 7.5 Ma (Fig. 7.15a). The folds are asymmetric, their northwestern slopes are steeper than southeastern ones. Axes of the folds display a downthrow towards southeast (Fig. 7.16a). Two anticlinal folds at the northeastern part of the area are divided by a graben which changes to a synclinal basin along its strike in the southwest (Fig. 7.16b). Thus, young tectonic fabric formed due to the 7.5 Ma intraplate deformation appears to be dominated by the NE-SW trending features at the polygon S22-III (Murthy et al. 1993b).

Third isopach map shows distribution of lowest pre-fan sediments draping basement (Fig. 7.16c). The thickness of the unit varies from 0.0 to 0.4s with the maximum thickness in the western part of the polygon. This map represents only the generalized structural style of pre-deformation oceanic crust as the basement could not be mapped undoubtedly all along the profiles. However, the tectonic fabric is very different from the overlying young one. Ancient tectonic features of basement appear to be rather in a N-S and E-W trend which suggests that they might have formed during spreading of seafloor in this part of the Indian Ocean.

### THE MK20 CRUISE MULTICHANNEL SEISMIC REFLECTION PROFILE

The published single-channel seismic reflection profiles certainly revealed the sedimentary structure in the Central Indian Ocean intraplate deformation area. But the basement could not be traced very clearly from